Geoelectric strike and its application in magnetotellurics

Mykola Khyzhnyak

Faculty of Earth Science
University of Iceland
2014

GEOELECTRIC STRIKE AND ITS APPLICATION IN MAGNETOTELLURICS

Mykola Khyzhnyak

10 ECTS thesis submitted in partial fulfillment of a
Bachelor Scientiarum degree in Geophysics

Advisor
Gylfi Páll Hersir

Faculty of Earth Science
School of Engineering and Natural Sciences
University of Iceland
Reykjavik, May 2014

Geoelectric strike and its application in magnetotellurics
10 ECTS thesis submitted in partial fulfillment of a B.Sc. degree in Geophysics

Faculty of Earth Science
School of Engineering and Natural Sciences
University of Iceland
Öskju, Sturlugötu 7
101, Reykjavik
Iceland

Telephone: 525 4600

Bibliographic information:
Mykola Khyzhnyak, 2014, Geoelectric strike and its application in magnetotellurics, B.Sc. thesis, Faculty of Earth Science, University of Iceland.

Printing: Háskólaprent, Fálkagata 2, 107 Reykjavík
Reykjavik, Iceland, May 2014

Abstract

Electrical resistivity methods in geophysical prospecting have been the most powerful tool in geothermal exploration. Determination of geoelectric strike angle in magnetotelluric (MT) measurements is a valuable contribution to an overall analysis of resistivity data. Among the applications of the strike analysis are the delineation of the boundaries of geothermal reservoirs and determination of fractures and faults at different depths which are the ideal flow paths of geothermal fluid. Strike analysis reveals complexity of resistivity structures within geothermal areas. Four MT soundings were conducted on Reykjanes peninsula in May 2014 and the data were compared with results of strike analysis from Krafla and Námafjall. Similarity in geoelectric strike behaviour in high-temperature areas confirms the results of inversion of resistivity soundings. The strike angle is found by rotation of the impedance tensor by a certain angle α which in turn minimizes diagonal tensor elements Z_{xx} and Z_{yy}.

Contents

List of Figures

Abbreviations and symbols

EM	-	Electromagnetic
MT	-	Magnetotelluric
TEM	-	Transient electromagnetics
ISOR	-	Iceland GeoSurvey
TM	-	Transverse magnetic (TM-mode)
TE	-	Transverse electric (TE-mode)
1D, 2D, 3D	-	one-, two- and three-dimensional
TS	-	Time series
TBL	-	Table file
PRM	-	Robust Parameter files
EDI	-	Electronic data interchange (file format)
m b.sl.	-	meters below sea level
E [V/m]	-	Electric field
H [A/m]	-	Magnetic field
B [T]	-	Magnetic induction
D [C/m^2]	-	Electric field
j [A/m^2]	-	Electric current density
Z [Ω]	-	Impedance tensor
R	-	Rotation matrix
W [Ω]	-	Wiese-Parkinson matrix (Tipper)
S	-	Skew-parameter of dimensionality
η [C/m^3]	-	Electrical charge density of free charges
μ [H/m]	-	Magnetic permeability
ε [F/m]	-	Electric permittivity
σ [S/m]	-	Electrical conductivity
ρ [Ωm]	-	Resistivity
ω [rad/s]	-	Angular frequency
i	-	Imaginary unit of a complex number
f [Hz]	-	Frequency
T [s]	-	Period of oscillation
θ	-	Phase angle
α	-	Swift-angle (Zstrike)
δ [m]	-	Penetration depth

Acknowledgments

I would like to thank my family and friends for their support during my academic years in the University of Iceland and especially my lovely wife for her patience during my studies.

My special thanks go to my advisor, Gylfi Páll Hersir, the geophysicist at Iceland GeoSurvey (ÍSOR). Despite being tremendously occupied in his office, his guidance and professionalism helped me with writing this thesis.

I would also like to thank Hjálmar Eysteinsson, the geophisicist at Reykjavík Geothermal, for his permission to use and display the results of the studies on geoelectric strike in the Krafla geothermal area.

1 Introduction

Electrical resistivity methods, particularly magnetotelluric (MT) and transient electromagnetic (TEM) methods, are common and the most powerful exploration techniques in geothermal exploration. These methods reveal valuable information on physical properties of geothermal reservoirs and applied to detect and map potential geothermal reservoirs and possible fractures beneath the surface. Interpretation of the data allows to delineate the boundaries of resistivity structure and determine rock resistivity and flow paths of geothermal fluid. The resistivity of rocks is influenced by alteration processes, temperature, fluid content, porosity, etc.

The fundamental theory of magnetotellurics was developed independently in the 1950 by Cagniard (1953) in France and by Tikhonov (1950) in the Soviet Union. MT method is a passive exploration method that involves measuring time variations in natural electric and magnetic field in order to determine the resistivity structure at depths. The signal source is the natural fluctuations of the Earth's magnetic field that induce an electric field in the ground. The signal is measured on the surface in two horizontal and orthogonal directions. The MT method has the greatest penetration depth among all electrical methods of exploration. The depth ranges from few hundreds of meters to tens of kilometers, depending on the frequency and quality of the data. The near-surface inhomogeneities in fact shift the resistivity curve in processing softwares and additional correction has to be applied. The effect is known as the static shift. For this purpose the TEM method is used for correction (Árnason et al., 2010).

The aim of this thesis is to study geoelectric strike and induction arrows from magnetotelluric data, its determination and application. Two studies on geoelectric strike were analysed and compared to MT measurements conducted on Reykjanes peninsula in May 2014 (figure 1.1). The direction along which the conductivity is constant is known as the geoelectric strike, or Zstrike. The strike angle is found by minimization of diagonal elements of impedance tensor It may represent a fracture or a fault with a flow path of geothermal fluid. Often, it coincides with geological fractures but sometimes depends on the resistivity pattern of the subsurface. However, Zstrike suffers from 90° ambiguity. Another way to represent resistivity distribution is a graphical introduction of induction arrows calculated from Wiese-Parkinson matrix, also known as Tipper (Wiese, 1962). Tipper does not suffer from 90° ambiguity and represents a clear picture on the strike direction. At low frequencies induction

arrows point away from a conductive zone and its distinctive characteristic allows to determine the boundary of geothermal reservoir or a fracture filled with geothermal fluid.

The geological strike direction in Reykjanes mainly follows the oblique rifting plate boundaries of American and Eurasian plate. The presence of high-temperature geothermal areas on the peninsula alters geoelectric strike direction at different depths. In comparison to strike directions from Krafla (Eysteinsson, 2010) and Námafjall (Karlsdóttir et al., 2012) geothermal areas, the geoelectric strike on the Reykjanes peninsula shows similar behaviour in the vicinity of geothermal reservoirs, i.e. the Tipper strike follows zones of anomalous resistivity rather than dominant geological strike. This work implies the analysis of geoelectric strike direction in MT measurements, its interpretation and application in further studies.

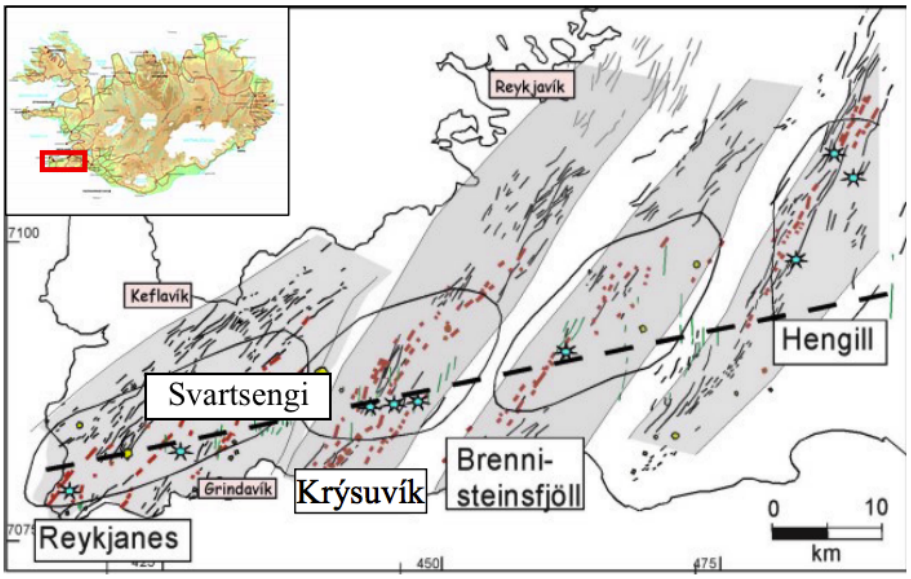

Figure 1.1: Tectonic map of Reykjanes peninsula showing fissure swarms, eruptive fissures and geothermal centres (Mawejje, 2007)

2 Magnetotelluric method

2.1 EM theory

The electromagnetic field within a material of a static reference frame is governed by Maxwell's equations. The time-varying magnetic field induces an electrical field in the medium. The magnetotelluric method is based on the following four equations which can be expressed in differential form as:

$$\nabla \times \mathbf{E} = -\frac{\partial \mathbf{B}}{\partial t} \tag{2.1a}$$

$$\nabla \times \mathbf{H} = \mathbf{j} + \frac{\partial \mathbf{D}}{\partial t} \tag{2.1b}$$

$$\nabla \cdot \mathbf{D} = \eta \tag{2.1c}$$

$$\nabla \cdot \mathbf{B} = 0 \tag{2.1d}$$

where $\mathbf{E}$ – electric field, $[V/m]$;
$\mathbf{H}$ –magnetic field, $[A/m]$;
$\mathbf{B}$ – magnetic induction, $[T]$;
$\mathbf{D}$ – electric displacement current, $[C/m^2]$;
$\mathbf{j}$ – electric current density, $[A/m^2]$;
η – electrical charge density of free charges, $[C/m^3]$.

In order to apply Maxwell's equation the relation between $\mathbf{E}$, $\mathbf{D}$, $\mathbf{B}$ and $\mathbf{H}$ has to be established. For isotropic medium such relation is specified by the constitutive equations:

$$\mathbf{B} = \mu \mathbf{H} \tag{2.2a}$$

$$\mathbf{D} = \varepsilon \mathbf{E} \tag{2.2b}$$

$$\mathbf{J} = \sigma \mathbf{E} \tag{2.2c}$$

Here, μ - the magnetic permeability measured in [H/m], ε - the electric permittivity [F/m] and σ - the electrical conductivity [S/m]. The reciprocal value of electrical

conductivity is resistivity, $\rho = 1/\sigma$, measured in $[\Omega m]$. Although the electrical conductivity appears in the constitutive equations, the resistivity is the commonly used parameter in magnetotellurics.

The variables μ, ε and σ are the properties depending entirely on the material through which the electromagnetic waves propagate. For homogeneous materials, ε and μ are constants while for inhomogeneous materials they depend on time and position within the material. In the case of isotropic material, μ and ε are scalars and for anisotropic materials they are represented by tensors. The variation in the resistivity of the earth is highly dependent on parameters that characterize the reservoir. These variations are related to the properties of interests and depend on porosity of the rock, alteration, water saturation, salinity of the water, temperature, etc.

The values of ε for most materials within the Earth vary between ε_0 which is the electric permittivity in vacuum and equals $8.85 \cdot 10^{-12}$ [F/m], and approximately $80\varepsilon_0$ - the electric permittivity of water (Keller, 1987). The magnetic permeability of most Earth materials can be approximated to its value in a vacuum, $\mu_0 = 4\pi \cdot 10^{-7}$ [H/m], but can be greater for highly magnetized materials. It's variation depends on temperature conditions of the reservoir and may appear due to decrease of the temperature below the Curie point, the temperature at which a material loses its ability to retain magnetism (Radhakrishnamurthy and Likhite, 1970).

2.2 The EM field in conductive media

In the case of a homogeneous and isotropic medium, substituting of equations (2.2) into equations (2.1) and assuming the harmonic dependance of the oscillating EM fields, $e^{i\omega t}$, leads to following relationships:

$$\nabla \times \mathbf{E} = -i\omega\mu\mathbf{H} \tag{2.3}$$

$$\nabla \times \mathbf{H} = (\sigma + i\omega\varepsilon)\mathbf{E} \tag{2.4}$$

where $\omega = 2\pi f$ - the angular frequency, $f = 1/T$ - the frequency of oscillation, T - the period of oscillation and $i = \sqrt{-1}$ - the imaginary unit of a complex number. There is no charge accumulation in a homogeneous conductive medium, therefore Gauss's law implies that $\nabla \cdot \mathbf{D} = \nabla \cdot (\varepsilon\mathbf{E}) = 0$. Considering the EM waves to be vertically incident plane waves only, it follows that $\nabla_x = \nabla_y = 0$ and the EM field has only z-component. Using the definition of *curl*, equations (2.3) and (2.4) give:

$$\frac{\partial E_z}{\partial y} - \frac{\partial E_y}{\partial z} = -i\omega\mu H_x \qquad (2.5a) \qquad \frac{\partial H_z}{\partial y} - \frac{\partial H_y}{\partial z} = (\sigma + i\omega\varepsilon)E_x \qquad (2.6a)$$

$$\frac{\partial E_x}{\partial z} - \frac{\partial E_z}{\partial x} = -i\omega\mu H_y \qquad (2.5b) \qquad \frac{\partial H_x}{\partial z} - \frac{\partial H_z}{\partial x} = (\sigma + i\omega\varepsilon)E_y \qquad (2.6b)$$

$$\frac{\partial E_y}{\partial x} - \frac{\partial E_x}{\partial y} = -i\omega\mu H_z \qquad (2.5c) \qquad \frac{\partial H_y}{\partial x} - \frac{\partial H_x}{\partial y} = (\sigma + i\omega\varepsilon)E_z. \qquad (2.6c)$$

Applying assumptions mentioned earlier, eqs. (2.5) and (2.6) become

$$\frac{\partial^2 E_x}{\partial z^2} = -i\omega\mu\frac{\partial H_y}{\partial z} = i\omega\mu(\sigma + i\omega\varepsilon)E_x \qquad (2.7a)$$

$$\frac{\partial^2 E_y}{\partial z^2} = \quad i\omega\mu\frac{\partial H_x}{\partial z} = i\omega\mu(\sigma + i\omega\varepsilon)E_y \qquad (2.7b)$$

Following a similar approach we find a relation for H_x and H_y:

$$\frac{\partial^2 H_x}{\partial z^2} = i\omega\mu\frac{\partial E_y}{\partial z} = i\omega\mu(\sigma + i\omega\varepsilon)H_x \qquad (2.8a)$$

$$\frac{\partial^2 H_y}{\partial z^2} = i\omega\mu\frac{\partial E_x}{\partial z} = i\omega\mu(\sigma + i\omega\varepsilon)H_y. \qquad (2.8b)$$

Equations (2.7) and (2.8) may be expressed as

$$\frac{\partial^2 E_{x,y}}{\partial z^2} = k^2 E_{x,y} \qquad (2.9)$$

$$\frac{\partial^2 H_{x,y}}{\partial z^2} = k^2 H_{x,y} \qquad (2.10)$$

where $k^2 = (i\omega\mu\sigma - \omega^2\mu\varepsilon)$ – the wavenumber of the EM wave. In a conductive medium, where $\sigma \gg \omega\varepsilon$, the wavenumber k represents the quasi-static approximation, or $k \approx \sqrt{i\omega\mu\sigma}$. The results above completely describe the electric and magnetic field in a homogeneous medium. A general solution to eqs. (2.9) and (2.10) is:

$$E_{x,y}(t) = (A_{x,y}e^{kz} + B_{x,y}e^{-kz})e^{i\omega t} \qquad (2.11)$$

$$H_x(t) = \frac{k}{i\omega\mu}(A_y e^{kz} - B_y e^{-kz})e^{i\omega t} \qquad (2.12)$$

$$H_y(t) = \frac{-k}{i\omega\mu}(A_x e^{kz} - B_x e^{-kz})e^{i\omega t} \qquad (2.13)$$

where $A_{x,y}$ and $B_{x,y}$ are constants to be determined from the boundary conditions. Since the EM field in MT measurements originates from the ionosphere it applies that all the quantities must remain finite when z goes to infinity. Thus the first terms in eqs. (2.11), (2.12) and (2.13) vanish:

$$E_{x,y}(t) = B_{x,y}e^{-kz}e^{i\omega t} \qquad (2.14)$$

$$H_x(t) = \frac{1}{i\omega\mu}\frac{\partial E_y}{\partial z} = \frac{-k}{i\omega\mu}B_y e^{-kz}e^{i\omega t} \qquad (2.15)$$

$$H_y(t) = \frac{-1}{i\omega\mu}\frac{\partial E_x}{\partial z} = \frac{k}{i\omega\mu}B_x e^{-kz}e^{i\omega t} \qquad (2.16)$$

The ratio between the orthogonal components of the electric and magnetic field intensity is known as the characteristic impedance, **Z**, and represents a characteristic measure of the EM properties of the subsurface. It has units of resistance, [Ω]. For a uniform earth, the surface impedance is related to the true resistivity of the rock. The ratio between the orthogonal component of electric and magnetic field yields the Tikhonov-Cagniard impedance:

$$Z_{xy} = \frac{E_x}{H_y} = \frac{i\omega\mu}{k} \approx \sqrt{\frac{\omega\mu}{\sigma}} e^{i\pi/4} \tag{2.17a}$$

$$Z_{yx} = \frac{E_y}{H_x} = \frac{-i\omega\mu}{k} = -Z_{xy} \tag{2.17b}$$

The dimensions of the electric and magnetic field intensity are $[V/m]$ and $[T]$, respectively, but it is common to measure these properties in $[mV/km]$ and $[\gamma = 10^{-9}nT]$. Equations (2.17) have a constant phase of $\theta = \pi/4$ and the magnetic field lags behind the electric field by 45° for a homogeneous Earth. The phase θ is independent of resistivity. According to Cagniard (1953) the conventional apparent resistivity is defined as:

$$\rho = \frac{1}{\omega\mu}|Z|^2, \quad [\Omega m] \tag{2.18}$$

Using eq. (2.2a), where $\mu = \mu_0$, and practical units for $E = E' \cdot 10^{-6}$ $[V/m]$ and $H = 1/\mu \cdot B' \cdot 10^{-9}$ $[A/m]$, the apparent resistivity may be represented by:

$$\rho = \frac{1}{\omega\mu}\left|\frac{E' \cdot 10^{-6}}{1/\mu \cdot B' \cdot 10^{-9}}\right|^2 10^6 = 0.2T\left|\frac{E'}{B'}\right|^2 \tag{2.19}$$

Hence, the resistivity is calculated from the orthogonal components of **E** and **H** and depends on the period of the EM wave, T. E' is measured in $[mV/km]$ and B' in $[\gamma]$.

For a homogeneous medium the resistivity is given by eq. (2.18) with a phase $\theta = \arg(Z) = \pi/4$. For a non-homogeneous medium an apparent resistivity, ρ_a, is defined and given by

$$\rho_a = \frac{1}{\omega\mu}|Z_0|^2 \tag{2.20}$$

where Z_0 is the impedance at the surface, with an apparent phase $\theta_a = \arg(Z_0) \neq \pi/4$.

2.3 Depth of penetration

In a uniform material the depth z to which EM waves penetrate is a function of frequency and the resistivity of the subsurface. The specific depth where the amplitude of the EM waves reduces to $1/e$ of its initial amplitude at the surface is

commonly referred to as skin depth or penetration depth, δ [m]. The penetration depth is described by the following:

$$\delta = 500\sqrt{\rho_a T} \quad [\text{m}] \tag{2.21}$$

where ρ_a - the resistivity of the structure. The penetration depth determines the investigation depth which increases as the square root of the material resistivity and period. Despite its definition of homogeneous media, eq. (2.21) may be applied to real geological structures.

2.4 Impedence tensor

The relation between electric and magnetic field, as shown in section 2.2, is described by the following equation which can be represented in a matrix form as:

$$\begin{bmatrix} E_x \\ E_y \end{bmatrix} = \begin{bmatrix} Z_{xx} & Z_{xy} \\ Z_{yx} & Z_{yy} \end{bmatrix} \begin{bmatrix} H_x \\ H_y \end{bmatrix} \tag{2.22}$$

or

$$\mathbf{E} = \mathbf{ZH} \tag{2.23}$$

The impedance $\mathbf{Z}$ is a complex tensor and is a function of the earth's resistivity (ρ). The solution to the MT problem simplifies to reconstruction of resistivity from the frequency dependence of $\mathbf{Z}$. The asymmetry of the material is given by on-diagonal components of $\mathbf{Z}$ in eq. (2.22). They become zero if the material is symmetric about a vertical plane passing through the observation site (Berdichevsky and Dmitriev, 2002). The off-diagonal components of $\mathbf{Z}$ give the information about vertical variations in resistivity structure. The spatial distribution of resistivity can be classified in three ways:

1D-Earth:

In the case of one-dimensional medium the resistivity changes with depth only. The impedance tensor $\mathbf{Z}$ can be written as

$$\mathbf{Z} = \begin{bmatrix} 0 & Z_{xy} \\ Z_{yx} & 0 \end{bmatrix} \tag{2.24}$$

where $Z_{xy} = -Z_{yx} \neq 0$. For 1D-Earth the apparent resistivity is given by

$$\rho_{xy} = \rho_{yx} = \frac{1}{\omega\mu}|Z|^2 \tag{2.25}$$

and the apparent phase is given by

$$\theta_{xy} = \theta_{yz} = \arg Z \tag{2.26}$$

which equals 45° for a homogeneous earth.

2D-Earth:

For two-dimensional earth resistivity varies with depth and in one horizontal direction. The direction in which the resistivity remains constant is called the geoelectric strike. The coordinate system can be rotated in such way that $Z_{xx} = Z_{yy} = 0$ but $Z_{xy} \neq -Z_{yx}$ (see section 2.6). The impedance tensor becomes:

$$\mathbf{Z} = \begin{bmatrix} 0 & Z_{xy} \\ Z_{yx} & 0 \end{bmatrix} \tag{2.27}$$

Although the eq. (2.27) is similar to eq. (2.24), the 2D-scenario requires that the components $|Z_{xy}|$ and $|Z_{yx}|$ are not equal. The rotation of $\mathbf{Z}$ involves the decomposition of the electric and magnetic field components into E-polarization (TE mode) and B-polarization (TM mode) as explained by Berdichevsky and Dmitriev (2008). In the TE mode the electric field is aligned with the electric strike and in the TM mode the magnetic field is aligned with the strike. If x-axis is in the strike direction, the off-diagonal components of eq. (2.27) become:

$$Z_{xy} = \frac{E'_x}{H'_y} \equiv Z_{TE}, \qquad \text{TE mode} \tag{2.28a}$$

$$Z_{yx} = \frac{E'_y}{H'_x} \equiv Z_{TM}, \qquad \text{TM mode} \tag{2.28b}$$

Often Z_{TE} is written as $Z^{\parallel}$, i.e. E_x is parallel to the strike, and Z_{TM} is written as $Z^{\perp}$, i.e. E_y is perpendicular to the strike. The apparent resistivity for each mode is then:

$$\rho_{xy} = \frac{1}{\omega\mu}|Z_{xy}|^2 = \frac{1}{\omega\mu}|Z_{TE}|^2 \tag{2.29a}$$

$$\rho_{yx} = \frac{1}{\omega\mu}|Z_{yx}|^2 = \frac{1}{\omega\mu}|Z_{TM}|^2 \tag{2.29b}$$

The phase angle in each mode is according to eq. (2.26) for each component separately:

$$\theta_{xy} = \arg Z_{xy}, \qquad \theta_{yx} = \arg Z_{yx} \tag{2.30}$$

3D-Earth:

In the 3D-Earth the variations in resistivity occur in all three directions. It follows that the impedance tensor is:

$$\mathbf{Z} = \begin{bmatrix} Z_{xx} & Z_{xy} \\ Z_{yx} & Z_{yy} \end{bmatrix} \tag{2.31}$$

where $Z_{xx} \neq Z_{yy} \neq 0$ and $Z_{xy} \neq Z_{yx}$. There is no way to rotate the impedance tensor in such way that on-diagonal elements of $\mathbf{Z}$ become zero.

2.5 Rotation of impedance tensor

Generally the axes of the coordinate system in the field layout do not coincide with the strike direction. The impedance tensor can be rotated to any other coordinate system by an angle α with the rotation matrix $\mathbf{R}$ and its transpose, $\mathbf{R}^T$. The angle of rotation is in a clockwise direction from the x-axis. The rotation operator is

$$\mathbf{R}(\alpha) = \begin{bmatrix} \cos\alpha & \sin\alpha \\ -\sin\alpha & \cos\alpha \end{bmatrix} \tag{2.32}$$

The new impedance tensor related to new axes, x' and y', and rotated by an angle α is given by

$$\mathbf{Z}(\alpha) = \mathbf{R}(\alpha)\,\mathbf{Z}\,\mathbf{R}(-\alpha) \tag{2.33}$$

The principle direction is defined as the direction when the off-diagonal components of $\mathbf{Z}(\alpha)$ are maximized after rotation. Maximizing $(|Z_{xy}(\alpha)|^2 + |Z_{yx}(\alpha)|^2)$ gives:

$$\alpha = \frac{1}{4}\arctan\frac{(Z_{xx}-Z_{yy})\overline{(Z_{xy}+Z_{yx})} + \overline{(Z_{xx}+Z_{yy})}(Z_{xy}-Z_{yx})}{|Z_{xx}-Z_{xy}|^2 - |Z_{xy}+Z_{yx}|^2} \tag{2.34}$$

where α is the resulting strike angle, also known as Swift angle (Swift, 1967). The other way to determine principle directions is to minimize the on-diagonal components of $\mathbf{Z}(\alpha)$ which yields the same result as in eq. (2.34).

2.6 MT strike analysis

Electrical strike reveals information about the directions in which the values of diagonal elements of impedance tensor come to a minimum. Often it is the same direction as the geological fractures. The layout of the measurements rarely coincides with the strike direction. In order to perform two-dimensional analysis of MT data the impedance tensor should be rotated by an angle α, as shown in section 2.5. The angle it makes with geographical north is the Swift angle (Swift, 1967). The rotation of $\mathbf{Z}$ by the angle α brings the impedance of the 3D-Earth close to 2D-model. The strike angle can be determined from eq. (2.34) with respect to the initial coordinate system. However, this approach implies the 90° ambiguity in the strike angle, so there is no way to distinguish between α and $(\alpha + 90°)$. The dimensionality of the structure is determined from the *skew*-parameter:

$$S = \left|\frac{Z_{xx}+Z_{yy}}{Z_{xy}-Z_{yx}}\right| \tag{2.35}$$

The large value of S indicates the three-dimensionality of the subsurface structure. For 1D-Earth the parameter S is zero and for 2D-Earth it should be close to zero after rotation of $\mathbf{Z}$.

Another way to determine the strike direction was introduced by Wiese (1962) and Parkinson (1983). The vertical component of magnetic field, H_z, may be expressed as a linear combination of horizontal magnetic field components, H_x and H_y. It is given by:

$$H_z = W_{zx}H_x + W_{zy}H_y \tag{2.36}$$

where $[W_{zx}\ W_{zy}] = \mathbf{W}$ is the Wiese-Parkinson matrix, also known as the *tipper*. The matrix $\mathbf{W}$ reflects the symmetry of the excess currents caused by horizontal distribution of resistivity. For 1D-model there are no induced currents in the vertical direction, therefore $\mathbf{W} = 0$. For 2D-Earth, the rotation of coordinate system places x-axis in the strike direction (also known as a T-strike) to minimize H_x and hence minimizing $|W_{zx}|$. Theoretically, during this transformation H_x becomes zero making $|W_{zx}| = 0$ which in turn implies maximization of $|W_{zy}|$. This approach does not suffer from 90° ambiguity.

Examples of T-strike from the Krýsuvík area in southwest Iceland for two period sets are shown in figure 2.1. The rose diagrams show the T-strikes for periods ranging from 0.01 s up to 100 s. As we see the low periods give the information on strike direction at shallow depths (see section 2.3). To the west of Vesturháls the electric strike is along the geological fracture. To the east of Vesturháls the strike direction seems to be randomly orientated but yet aligns dominant strike directions marked with red lines. Two dominant electric strikes in a zone between Vesturháls and Sveifluháls are perpendicular to geological fractures and indicate the main resistivity

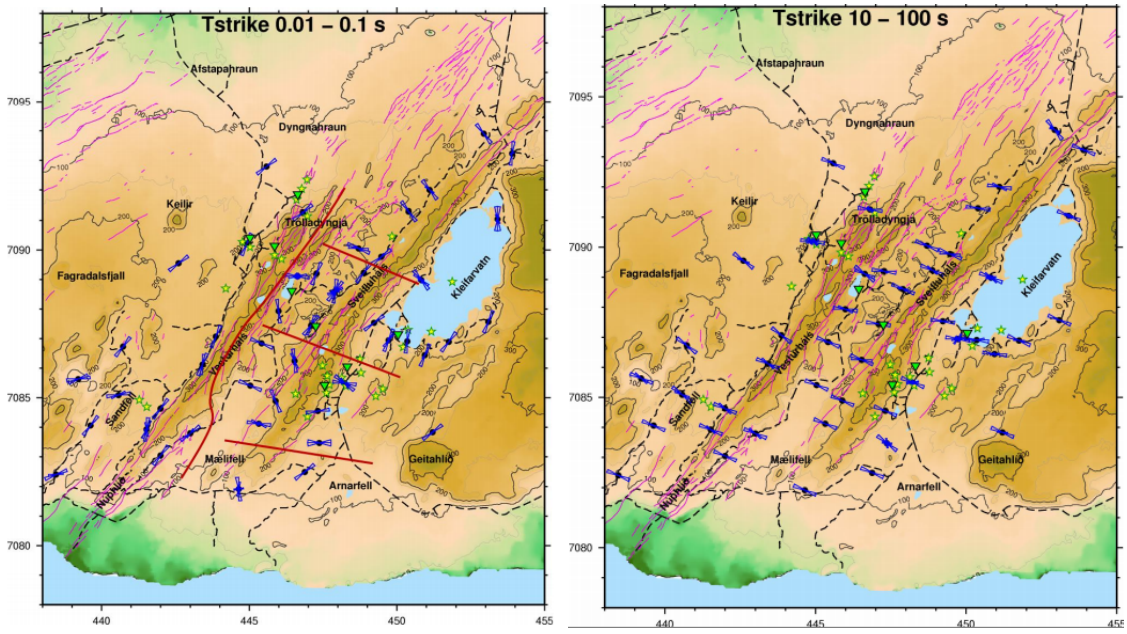

Figure 2.1: Rose diagrams of the Tipper strike for two period ranges, $0.01 - 0.1s$ *and* $10 - 100s$*, from Krýsuvík area in Southwest Iceland. (Hersir et al., 2011). Red lines indicate zones of different dominant strike directions.*

contrasts. Higher periods show the dominance of SE-NW geoelectric strike direction at great depths. For these periods the Tstrike is parallel to the coast, i.e. parallel to the resistivity gradient. The tipper vector consists of a real and imaginary part and can be represented by two real vectors, or induction arrows, and two imaginary vectors. At higher periods induction arrows point away from a conductive zone (Berdichevsky and Dmitriev, 2002) allowing the identification of conductive structure. In figure 2.2 induction arrows at lower periods are chaotically distributed near small resistivity structures but with increasing period they are pointing towards the zone of higher resistivity and away from the coast if the survey area lies in the vicinity of marine environment (Hersir et al., 2011).

The geoelectric strike is a function of frequency (the reciprocal value of the period) and changes with depth. It gives valuable information about highly permeable subsurface fractures which is often the pathways of geothermal fluid. In general the strike analysis shows consistency with the results of inversion of resistivity soundings and become a tool for indication of anomalous resistivity structures.

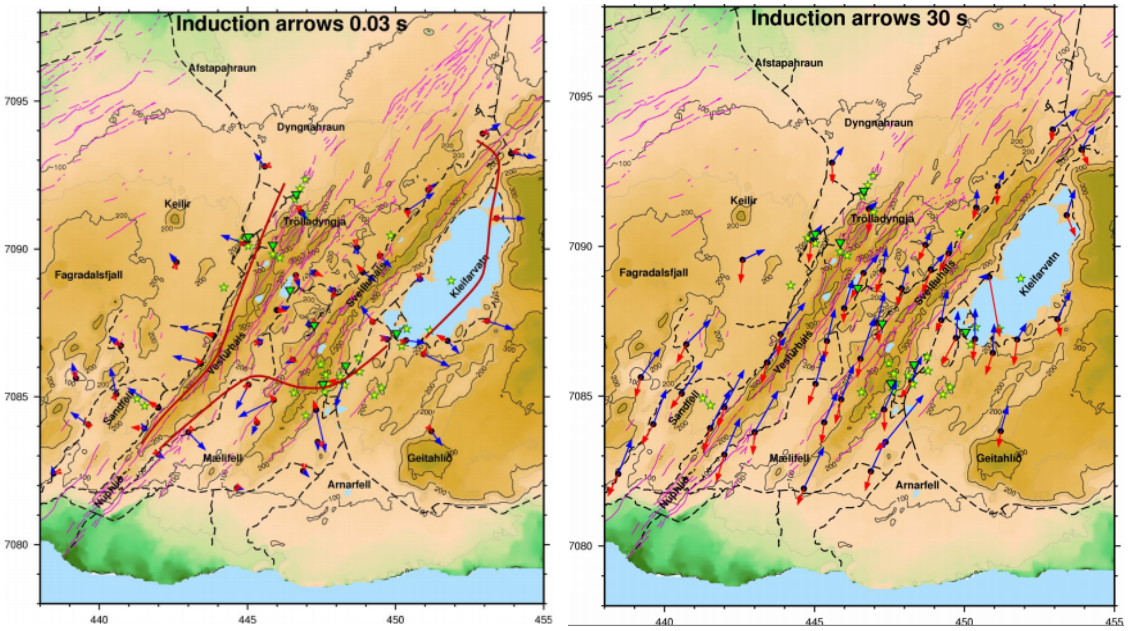

Figure 2.2: Induction arrows for the periods of 0.03*s and* 30*s from Krýsuvík area in Southwest Iceland (Hersir et al., 2011). Blue arrows denote the real part and red arrows the imaginary part. Red lines represent the boundaryies of a good conductor according to the arrows.*

2.7 The effect of static shift

The MT method, that measures an electric field on the surface, suffers from the telluric or static shift problems. The effect of static shift occurs due to the presence of small-scale near-surface inhomogeneities and it appears as a vertical shifting of the apparent resistivity curve by a frequency independent factor without any change in the phase curve (Sasaki, 2004). Jiracek (1990) proposed that the shift is caused by resistivity inhomogeneities in the vicinity of surveyed area and especially close to the electrical dipoles. The reasons are the voltage distortion of the electric field by highly conductive minerals, topographic distortion and current channeling. The voltage distortion occurs as a result of local resistivity anomaly near the surface, the topographic distortion takes place under the hills and valleys affecting the current density and the current channeling occurs when the current is deflected by resistivity anomaly. Jiracek (1990) gives an overview of the static shift problem and purposes the methods for its correction.

The static shift problem is common in geothermal areas in volcanic regions and must be corrected before MT data inversion. To do this, the transient electromagnetic measurements (TEM) are conducted at the same site with MT sounding (Sternberg et al., 1988). TEM does not suffer from static shift problem because the measured signal is the decaying magnetic field while the measured signal in MT is an electric field. Hence, joint inversion of TEM and MT data is used for static shift correction and the construction of a correct model for the area (Árnason et al., 2010).

2.8 Importance of a remote reference station

The MT data may be affected by cultural noise that is present at or near the survey area. It may be the highway nearby, the factories, the inhabited areas, etc. Gamble et al. (1979) suggested that it is appropriate to keep one station recording continuously at fixed location far away from the surveyed area. During the processing of the MT data the apparent resistivity curve gets biased down at high frequencies due to the presence of noise in the components of $\mathbf{H}$. Thus, eq. (2.19) results in reduced value of ρ_a. The remote reference station allows better quality data from the processing and higher signal to noise ratio.

3 Data acquisition and processing

3.1 MT setup

Four MT soundings were conducted on Reykjanes peninsula from 5th to 7th of May 2014, three soundings near Svartsengi high-temperature area and one in Reykjanes high-temperature area. The base station was installed on 5th of May in few kilometers from the surveyed area and all equipment was calibrated. The data were collected using 5-channel acquisition system manufactured by Phoenix Geophysics (figure 3.1). MTU data logger digitizes the analogue signal and synchronizes the time through the GPS-antenna. The synchronization allows the simultaneous installation of multiple MTU units at different sites without any interconnecting cables. GPS synchronization also permits the installation of remote reference station allowing noise reduction during processing. The typical setup of MT station is shown in figure 3.2. The electric field components, E_x and E_y, were measured on the surface in orthogonal directions by the pairs of non-polarized electrodes with porous ceramic base, filled with lead-chloride solution. The electrodes were connected to the data logger by coaxial cables. Preferably, the x-direction should be aligned with magnetic north as suggested by Hersir et al. (2013). The distance between two dipoles was approximately 50 m. For better contact with the ground and minimal temperature variations electrodes were buried at 30-40 cm depth and conductive absorbent (bentonite) was attached to the base to increase the area of contact. E_x and E_y were determined by measuring the potential difference, ΔV, between the dipoles. The measured potential difference is in order of magnitude $10^{-3} V$ and is very sensitive to wind noise, thus the cables were placed on the ground to reduce wind disturbance and covered where possible. Two horizontal components of magnetic field, H_x and H_y, were measured with the same

Figure 3.1: Phoenix V5 2000 MTU system (www.phoenix-geophysics.com).

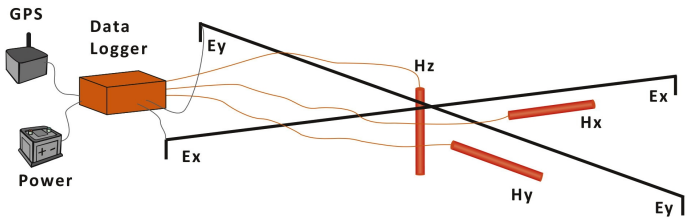

Figure 3.2: The field layout of a 5-channel magnetotelluric sounding. With courtesy of ÍSOR

alignment as E_x and E_y, but the vertical component of magnetic field, H_z, should be installed with the least deviation from the vertical line. A level bar is needed for proper installation of coils both in horizontal and vertical positions. H_x, H_y and H_z, were measured by induction coils. Due to their sensitivity to any external noise, coils were placed into the ground at a depth of 30-40 cm. It also secures coils from being affected by diurnal temperature variations. Such setup of the coils prevents any unnecessary movements.

MTU stores data on a removable memory card and then it is transferred to a computer where the data are processed. The total recording time at each site was approx. 20-24 hours. The electric and magnetic field is measured as a function of time. An example of time-series record of MT sounding is shown in figure 3.3.

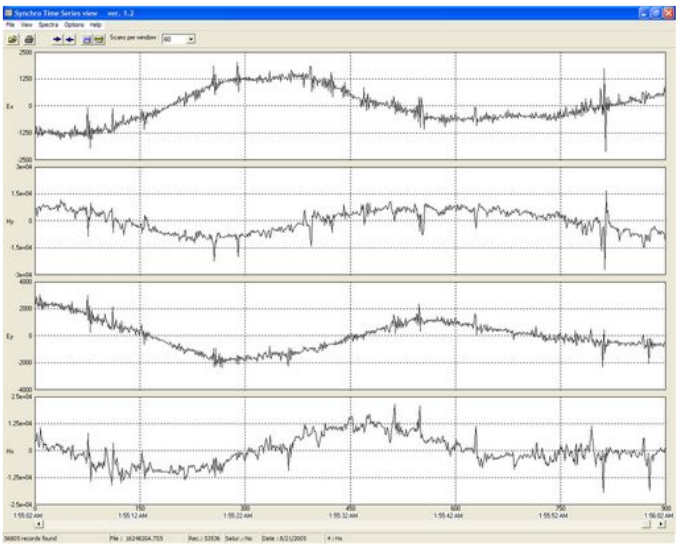

Figure 3.3: An example of MT time series during an interval of one minute. From top to the bottom are: E_x, H_y, E_y and H_x. Time series contain many different frequencies giving through processing resistivity as a function of period, using Fourier transformation.

3.2 Data processing

In processing MT data two softwares are used, supplied by Phoenix Geophysics, SSMT2000 and MTEditor. First, the data files from a memory card in the data logger transferred to the computer. The built-in option in SSMT2000 allows to preview raw time series (TS) data as shown in figure 3.3 and assess the quality of the data. The parameter file, or Table file (TBL), is generated from a startup file and constitute a record of all the parameters associated with the time series. It should be reviewed and, if necessary, updated before further proceeding. For example, if the dipole length is changed, the coils are substituted, etc. Any changes made before measurements should be added manually to startup file, a file that includes information on coils, calibration settings, default dipole length, sampling frequency, etc. Following that, the TS for each site are transformed from the time domain into the frequency domain (TS to FT). Figure 3.4 shows the interface of SSMT2000 software. The next step is to set up robust parameters (PRM) for each processing stage. These parameters are specific for each site.

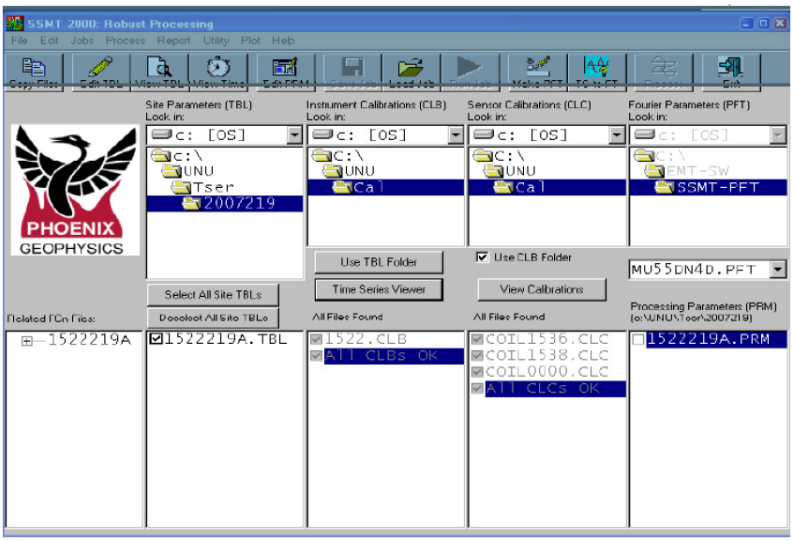

Figure 3.4: The SSMT2000 main window. Fourier transform of the MT time series is done by TStoFT option after the all necessary updates in TBL file.

After processing two types of files are created that are input files into MTEditor, ∗.mth and ∗.mtl, which contain information on Fourier coefficients for time series and crosspower and autopower density matrices. It plots resistivity and phase curves as a function of frequency using crosspowers and autopowers to calculate each value of resistivity and phase. MTEditor allows further refinement of data manually by masking outliers on resistivity or phase curves. The software also gives an information on tipper magnitude, strike direction for each frequency and coherency between the electric and magnetic field. If results are satisfactory the files are exported in a

standard EDI format suitable for use with other geophysical softwares. An example of resistivity and phase curves in MT Editor is shown in figure 3.5. EDI-files are the input files for the inversion operation carried out in Linux-based softwares.

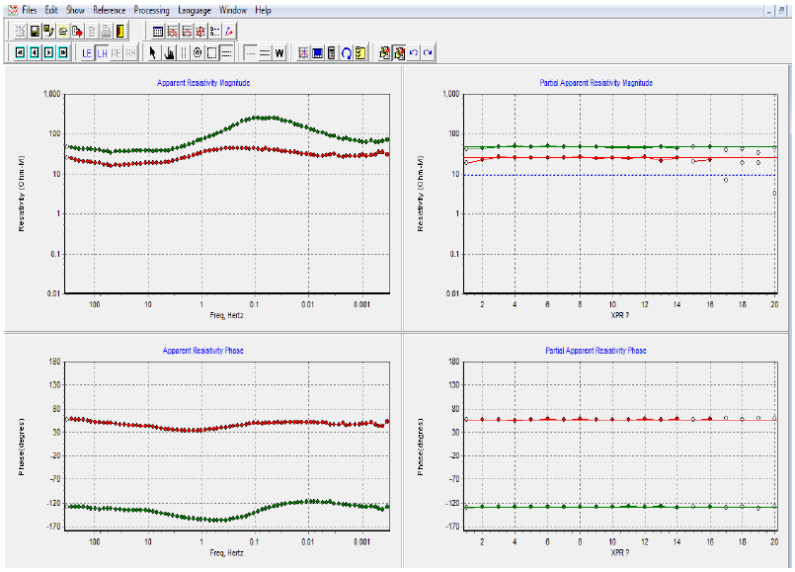

Figure 3.5: MT Editor main window. The resistivity and phase curves are shown on the left side. Each point on the resistivity and phase curves is a weighted average of 20 points shown to the right.

After the procedure listed above the output files are ready for inversion. File format ∗.EDI is and input in a programme, called TEMTD, for 1D inversion of MT and TEM data written by Knútur Árnason (2006). TEMTD invert MT and TEM data and also perform joint inversion of the data to determine the static shift parameter from the MT data. Other programmes, written by ISOR specialists, allow to calculate impedance tensor, its rotation, induction arrows, etc.

4 Strike analysis from Krafla and Námafjall

In this chapter the short analysis of geoelectric strike (see section 2.6) from Krafla and Námafjall geothermal areas is presented. The data are based on MT measurements conducted in the vicinity of Námafjall in 2009 (Karlsdóttir et al., 2012) and in Krafla between 2004 and 2007 (Eysteinsson, 2010). The results were published in reports prepared by Iceland GeoSurvey (ÍSOR) for Landsvirkjun, the national power company of Iceland.

4.1 Data from Krafla geothermal area

Around 170 measurements were conducted in the Krafla geothermal area between 2004 and 2007. It was a pioneer work on the determination of the geoelectric strike in this area. Most of the measurements (106) were done by Landsvirkjun in collaboration with Duke University is United States, another 55 measurements were conducted by the University of Moscow. ÍSOR did 6 MT-measurements in summer 2007.

Analysing the strike direction in surveyed area we look at the results showing Tskrike directions for periods 0.01-1 s and induction arrows for a period of 1 s (figures A.1 and A.2). According to Eysteinsson (2010) the Tstrike for periods 0.01-1 s and 1-100 s are very similar. Rose diagrams of Tstrike north and east of Víti are mostly orientated towards northwest which is nearly perpendicular to the dominant geological fractures. For higher periods the tipper has northward trend. The above-mentioned is a strong indication of the conductive pattern below Víti and indicates the dominance of geoelectric strike over geological strike.

The size of induction arrows varies mostly in the period range 0.1-10 s, indicating 2D or 3D resistivity structure at depths for corresponding frequencies. Below that depth the structure is close to 1D. Figure A.2 shows induction arrows for the period of 1 s. The direction of real vectors in the northeastern side of the caldera has a strong trend in NE indicating a good conductor lying in the opposite direction. The

arrows west of Víti are not as pronounced as in northeastern side. Notice how the most western induction arrows are pointing inward caldera indicating a possibly low resistivity zone behind the western caldera rim. Apparently, the size and direction of induction arrows reveal the complexity of the resistivity structure in the Krafla geothermal zone where 3D resistivity structure is present. In general the direction of the arrows is to NE for most periods.

4.2 Data from Námafjall geothermal area

Figures 4.2a and 4.2b represent Tipper strike for periods 0.01-0.1 s and induction arrows for period 0.3 s, respectively. Low resistivity is prominent below Námafjall as the rose diagrams of the Tipper strike (fig. 4.2a) encircle the geothermally altered area around the mountain. This is supported by resistivity map at 2000 m b.sl. in figure 4.1 (Karlsdóttir et al., 2012). Further south, the direction of Tstrike is dominated by geological fractures, reflecting the conductivity in fractures. At all MT sites in the vicinity of Námafjall Tipper vectors point away from the zone of low resistivity showing a fairly good directional trend in the data. The induction arrows shown in figure 4.2b in addition to Tipper strike are in strong correlation with resistivity map and reveal the ability of the MT method to clearly define resistivity structures at depths.

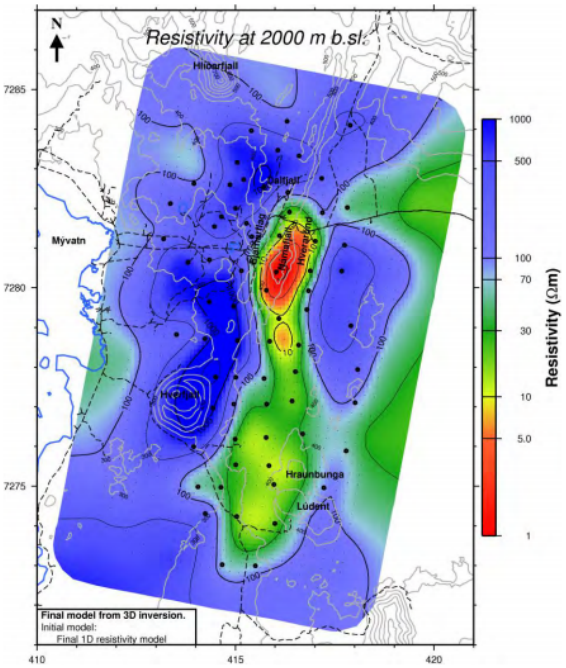

Figure 4.1: Resistivity at 2000m b.sl. (Karlsdóttir et al. (2012))

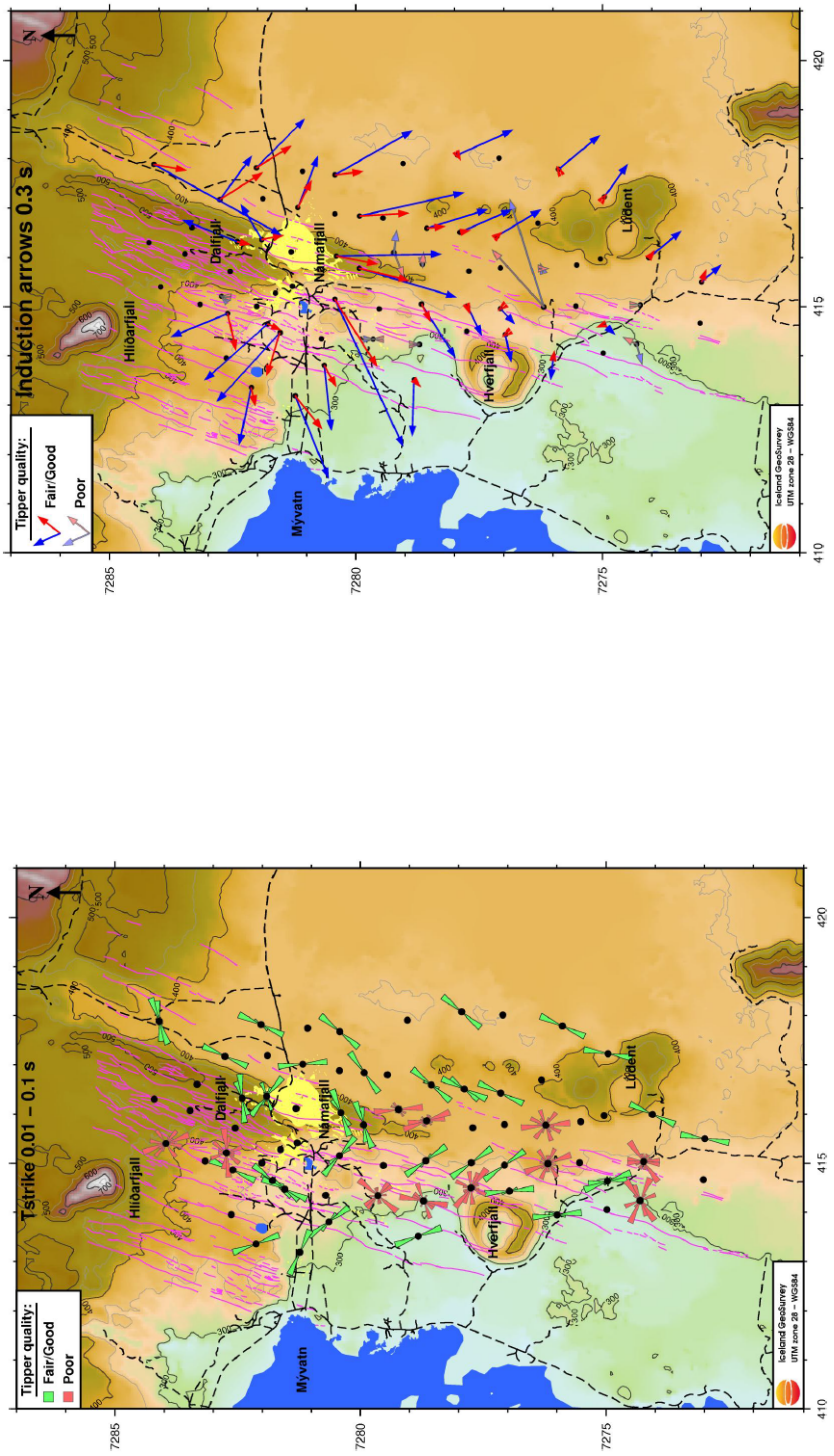

(a): Tipper strike *(b): Induction arrows*

Figure 4.2: Rose diagram of the (a) Tipper strike for periods 0.01-0.1 s and (b) induction arrows for the period 0.3 s. Fractures and faults are shown in magenta, blue arrows in (b) denote real part of the induction arrows and red arrows denote the imaginary part (Eysteinsson, 2010; Karlsdóttir et al., 2012).

5 Strike analysis from measured data in Reykjanes peninsula

Four soundings conducted during field work in Reykjanes were analysed. Unfortunately, only one out of four measurements was done with a use of vertical coil. Therefore, the calculation of induction vectors was possible only for one sounding. Figures A.3 - A.6 show processed data of all soundings. The analysis will mostly concern sounding chi002 where the tipper information is available. Figures A.4 and A.6 seem to represent fairly good results in comparison to other two soundings. Analysis of Zstrike and dimensionality parameters of Skew in figure A.4 implies that the subsurface structure does not show three-dimensional pattern. Zstrike, or Swift angle, is nearly constant throughout all frequency range and its direction is N15°W or N75°A due to 90° ambiguity. It applies that the geoelectic strike has directions NNW-SSE or ENE-WSW. There is no resistivity anomaly causing the change in strike direction and the dimensionality variable, *Skew*, is close to zero means that the resistivity structure is close to 2D (see section 2.6). The coherency of the data is poor in the dead-band, a frequency range where measurements suffer from bad data. According to Tipper at low periods the response of the earth is close to 2D-Earth as T_x is very close to zero but starting from a period of 1 s it slowly shows the 3D influence. Induction arrows of the sounding chi002 are shown in figure 5.1. As seen in figure the arrows are very small for small periods but increase rapidly in size with increasing depth. Taking into account Zstike and dimensionality variables for this sounding and the presence of the ocean the behavior of induction arrows at depth may be explained by the presence of salt water (Hersir et al., 2011).

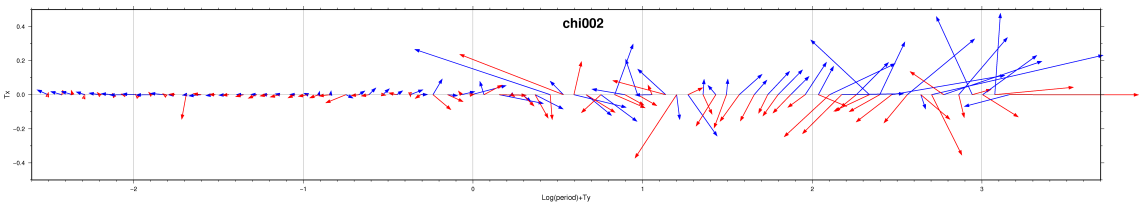

Figure 5.1: Induction arrows of MT sounding chi002 calculated from the available informaion on tipper shown on a log scale as a function of frequency. Blue arrows denote real part and red arrows denote imaginary part.

Skew in figure A.6 shows a clear indication of 3D resistivity structure in the period range 0.01-1 s. The Skew curve reaches the value of 0.7 which is a good indicator of three-dimensionality. For this sounding Zstrike is not constant and changes from being N60°W at lowest periods to almost N-direction at 1 s. However, there is still 90° ambiguity in strike direction and without having information on Tipper this problem remains unsolved. The coherency of the data from chi004 is good even in the dead-band region but it is biased down at low periods.

The data from chi001 (figure A.3) is very poor and should not be considered in further interpretation. The coherency is very scattered throughout all period range which indicates a very poor correlation between the electric and magnetic field. Despite that, there are still some signs of 3D structure coming from the Skew graph. The Zstrike is constant at low periods, corresponding to the depth of 1-2 km, but becomes scattered at higher periods.

6 Conclusion

The geoelectric strike analysis from Krafla, Námafjall and Reykjanes geothermal areas showed consistency in strike directions in different zones of geothermal areas. Resistivity anomalies formed by geothermal activity alter the direction of the electric strike and induction arrows. Unfortunately, the data for the vertical component of the magnetic field were not available for most of the soundings but one. The deficit of available quality data entails difficulties in the analysis of geoelectric strike. Nevertheless, the comparison of the one sounding from Reykjanes with results from Námafjall and Krafla geothermal area shows consistency of results and confirms the inversion model of resistivity measurements.

The electric strike direction reveals fractures and faults which are the flow path of geothermal fluid. The strike angle is found by mathematical operation when the diagonal elements of the impedance tensor, $|Z_{xx}|$ and $|Z_{yy}|$, are minimized. The induction arrows are the results of decomposition of tipper vector and indicate the direction of resistivity gradient. Induction arrows point away from zones of lower resistivity towards zones of higher resistivity giving a valuable information for further mapping of conductive paths within subsurface resistivity structures. The strike analysis of Krafla and Námafjall showed that in some distance from resistivity anomaly the Tstrike aligns dominant geological fractures and faults whereas around or within the geothermal areas the Tstrikes follow the boundaries of geothermal reservoirs or conductive paths.

In general, the directions observed in geoelectric strikes are mostly coincide with the dominant geological strike but when it comes to the presence of geothermal reservoirs or alteration zones within geothermal areas, the strike shows totally different behaviour, indicating the boundaries of the structures. It confirms the resistivity structures already revealed by inversion of resistivity soundings.

Bibliography

Árnason, K., Eystensson, H., and Hersir, G. P. (2010). Joint 1D inversion of TEM and MT data and 3D inversion of MT data in the Hengill area, SW Iceland. *Geothermics*, 39:13–34.

Berdichevsky, M. N. and Dmitriev, V. (2002). Magnetotellurics in the context of the theory of ill-posed problems. *Society of Exploration Geophysicists*, page 215.

Berdichevsky, M. N. and Dmitriev, V. I. (2008). Models and methods of magnetotelurics. *Sprinkler*, page 561.

Cagniard, L. (1953). Basic theory of the Magnetotelluric method of geophysical prospecting. *Geophysics*, 18:605–635.

Eysteinsson, H. (2010). Rafstrikstefnur í MT-mælingum á Kröflusvæði [Geoelectrik strike in MT measerements from Krafla geothermal area]. Lv-2010/082, Landsvirkjun.

Gamble, T. D., Goubau, W. M., and Clarke, J. (1979). Magnetotellurics with a remote magnetic reference. *Geophysics*, 44:53–68.

Hersir, G., Árnason, K., and Vilhjálmsson, A. M. (2011). 3D inversion of MT data from Krýsuvík, SW Iceland. *Report ÍSOR-2011/072*, page 165.

Hersir, G. P., Árnason, K., and Vilhjálmsson, A. M. (2013). 3D inversion of magnetotelluric (MT) resistivity data from Krýsuvík high temperature geothermal area in SW Iceland. *Thirty-Eights Workshop on Geothermal Reservoir Engineering*.

Jiracek, G. R. (1990). Near-surface and topographic distortion in electromagnetic induction. *Surveys in Geophysics*, 11:163–203.

Karlsdóttir, R., Beyene, A. T., and Vilhjálmsson, A. M. (2012). Námafjall geothermal area, Northern Iceland. 3D inversion of MT and TEM data. Lv-2012/112, Landsvirkjun.

Keller, G. V. (1987). Resistivity characteristics of geological targets. In *Electromagnetic methods in applied geophysics*, pages 13–15, Tulsa, Oklahoma.

Mawejje, P. (2007). Geothermal exploration and geological mapping at Seltún in Krýsuvík geothermal field, Reykjaes peninsula, SW Iceland. *Geothermal training programme*, (12).

Parkinson, W. D. (1983). *Introduction to geomagnetism.* Scottish Academic press, London.

Radhakrishnamurthy, C. and Likhite, S. D. (1970). Hopkinson effect, blocking temperature and Curie point in basalts. *Earth Planet Science Letters*, 7:389–396.

Sasaki, Y. (2004). Three-dimensional inversion of static-shifted magnetotelluric data. *Earth Planets Space*, 56:239–248.

Sternberg, B., Washburne, J. C., and Pellerin, L. (1988). Correction for the static shift in magnetotellurics using transient electromagnetic soundings. *Geophysics*, 53:1459–1468.

Swift, C. M. (1967). *A magnetotelluric investigation of an electric conductivity anomaly in the south-western U.S.* PhD thesis, MIT.

Tikhonov, A. N. (1950). The determination of electrical properties of the deep layers of the Earth's crust. *Doklady Akademii Nauk SSSR*, 73:293–297 (in Russian).

Wiese, H. (1962). Geomagnetische Tiefentellurik. *Geofis. Pura. Appl*, 52:83–103.

Appendix

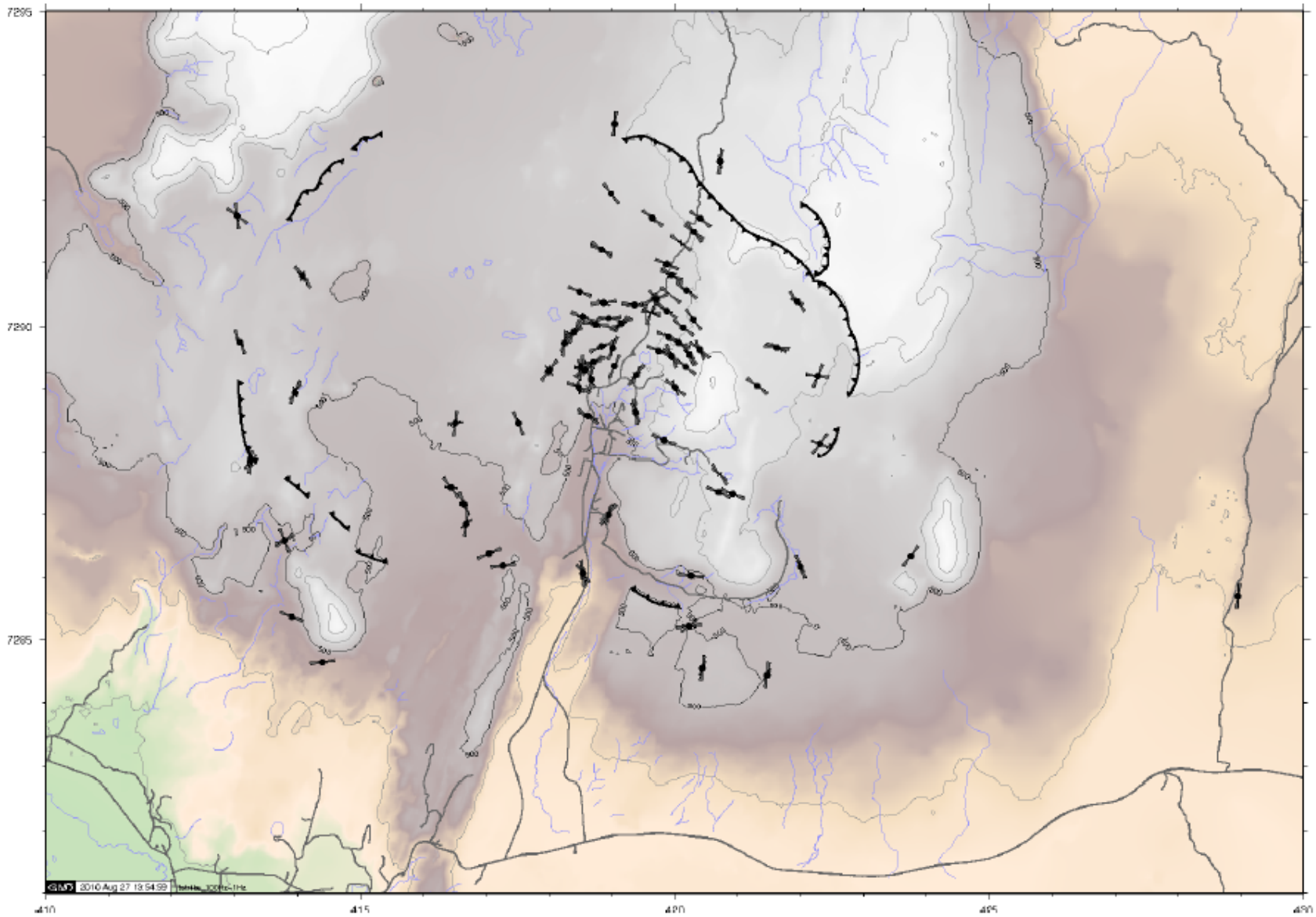

Figure A.1: Rose diagrams for the Tipper strike (Tstrike) for the period range 0.01-0.1 s.

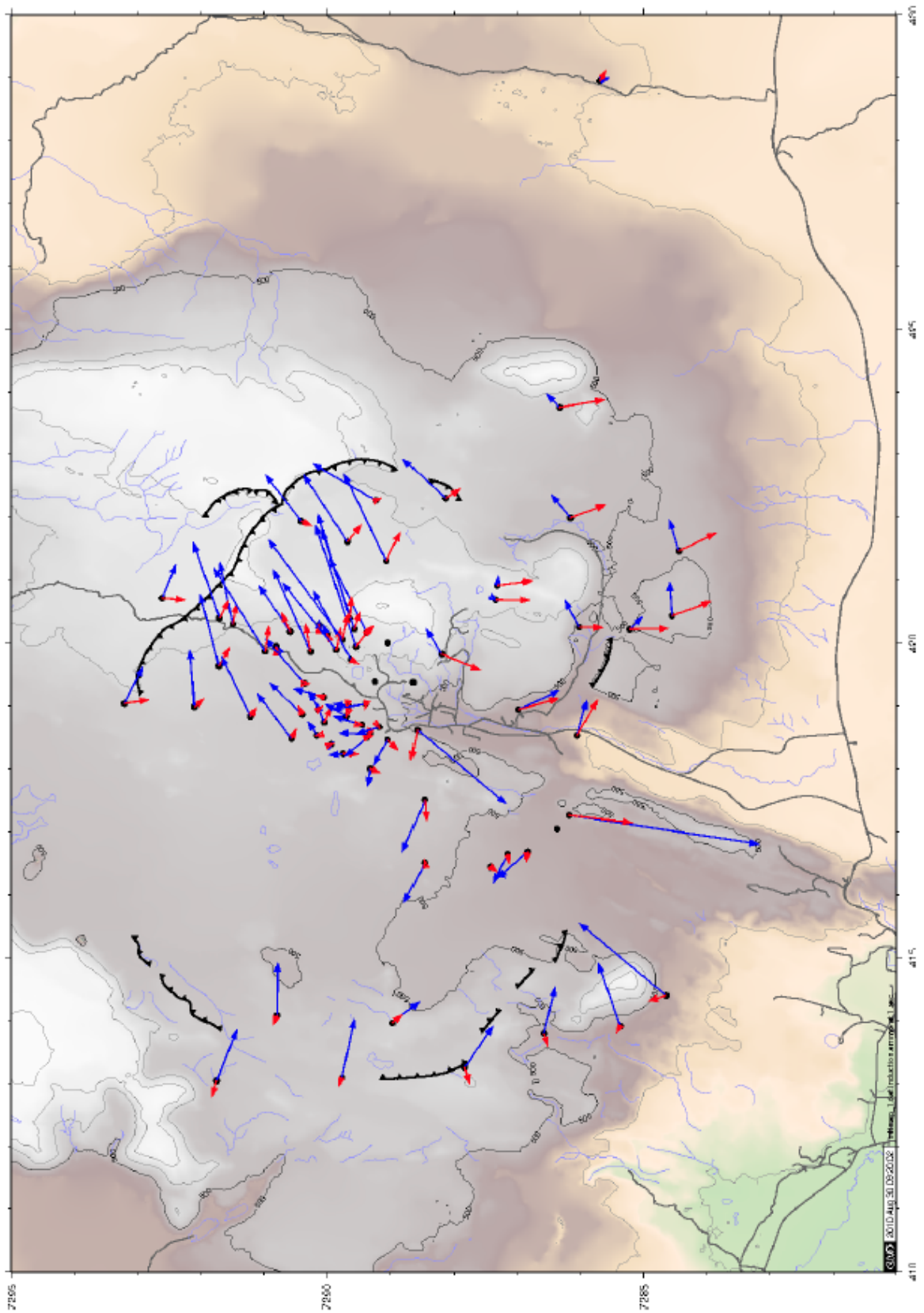

Figure A.2: Induction arrows for the period 1 s. Blue arrows denote real part and red arrows the imaginary part.

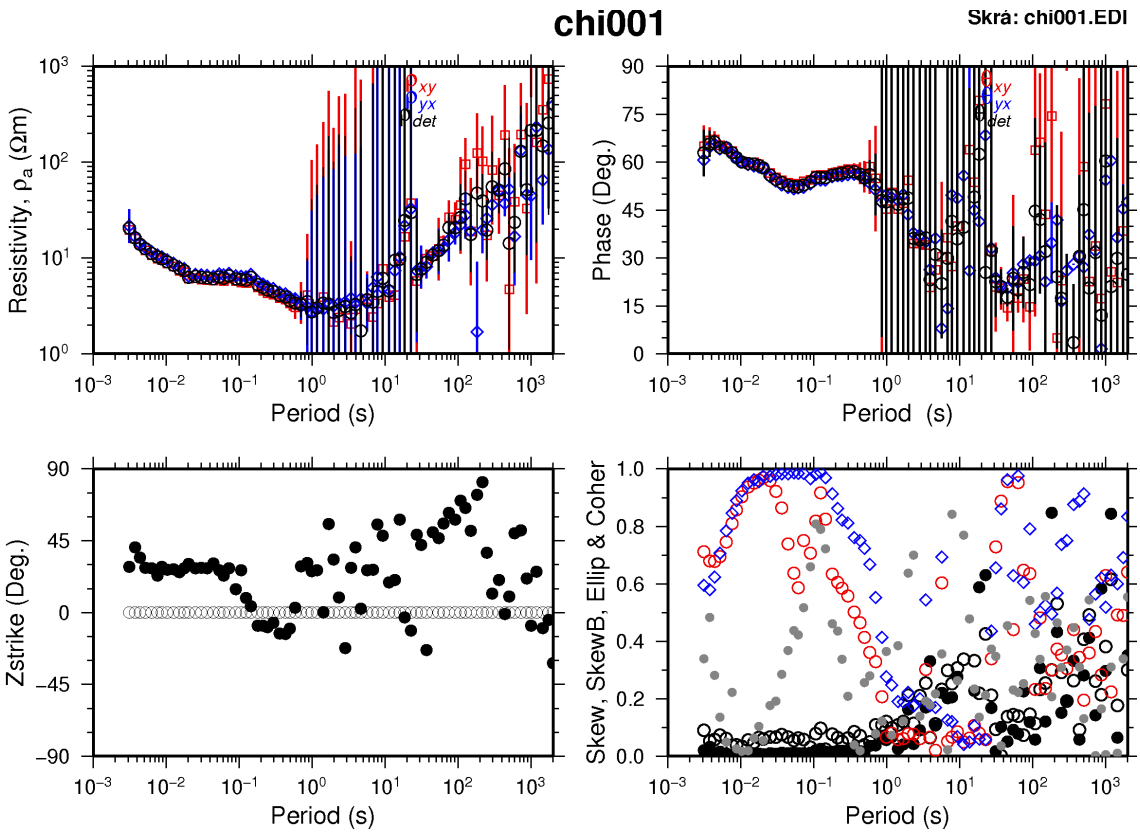

Figure A.3: Processed MT data for sounding chi001 from the Reykjanes high-temperature geothermal area. All measurements are functions of period. In the top to the left is the apparent resistivity and to the right is the phase angle. The second line to the left shows Zstrike for all periods and to the right are dimensionality variables, Skew, SkewB, Ellipticity and Coherency. These variables equal to zero for 1D and 2D structures. The last four figures correspond to Tipper. These data do not contain information on Tipper because vertical component of magnetic field, H_z, was not measured.

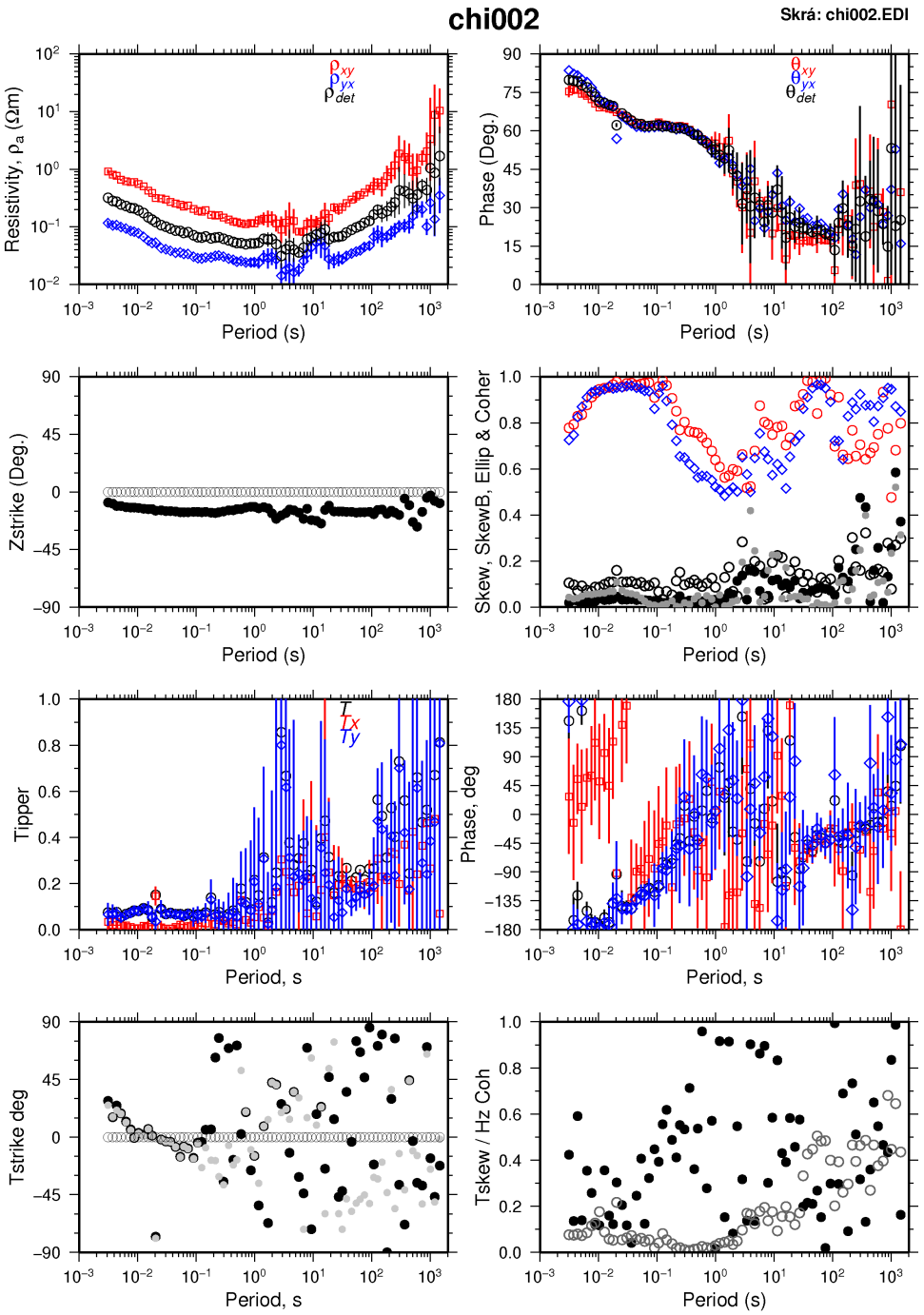

Figure A.4: Processed MT data for sounding chi002 from the Reykjanes high-temperature geothermal area. All measurements are functions of period. In the top to the left is the apparent resistivity and to the right is the phase angle. The second line to the left shows Zstrike for all periods and to the right are dimensionality variables, Skew, SkewB, Ellipticity and Coherency. These variables equal to zero for 1D and 2D structures. The last four figures correspond to Tipper. In third line to the left is the size of the Tipper and to the right its phase. The last line show the geoelectric strike direction to the left according to the Tipper and to the right is the dimensionality variable Tskew.

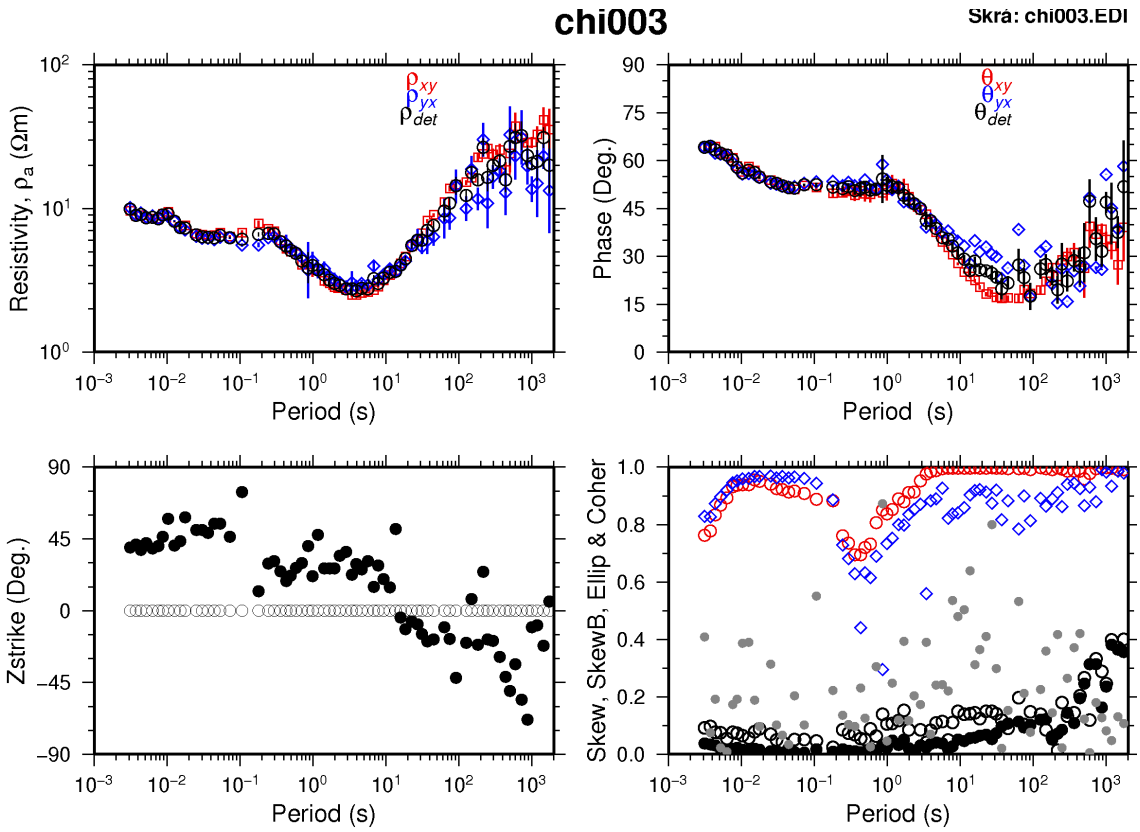

Figure A.5: Processed MT data for sounding chi003 from the Reykjanes high-temperature geothermal area. All measurements are functions of period. In the top to the left is the apparent resistivity and to the right is the phase angle. The second line to the left shows Zstrike for all periods and to the right are dimensionality variables, Skew, SkewB, Ellipticity and Coherency. These variables equal to zero for 1D and 2D structures. The last four figures correspond to Tipper. These data do not contain information on Tipper because vertical component of magnetic field, H_z, was not measured.

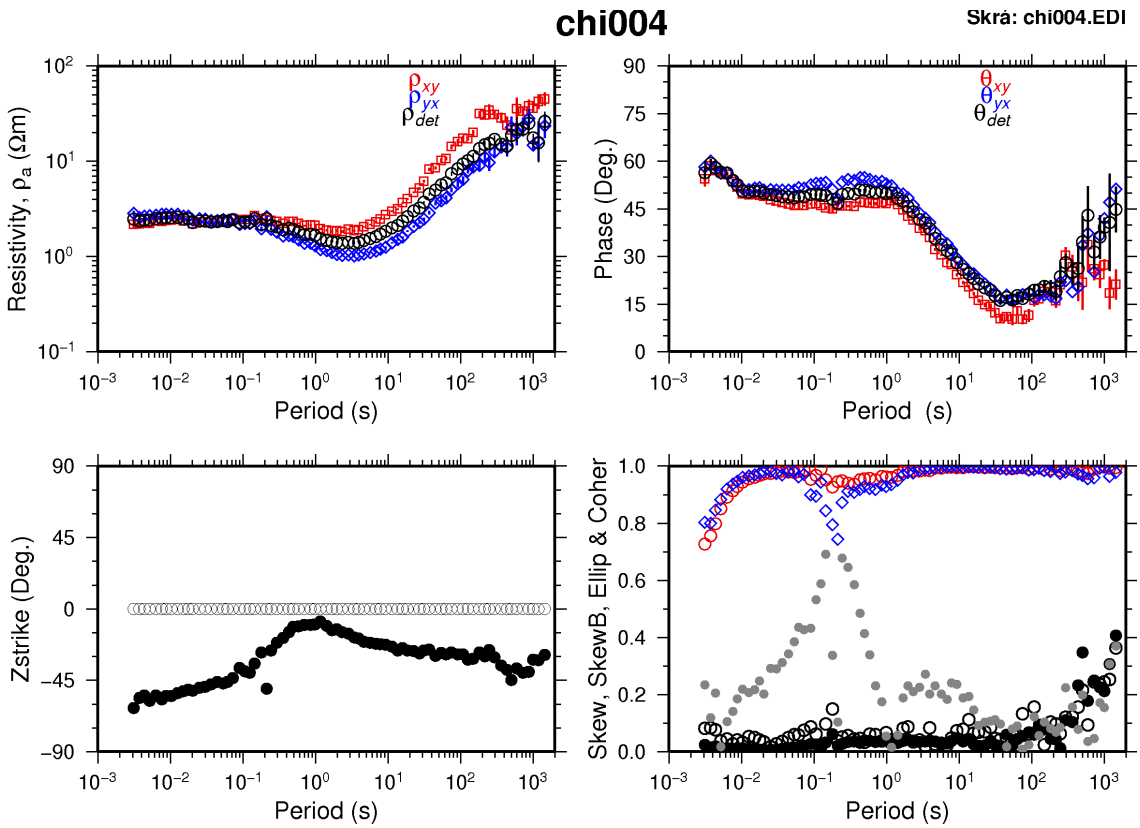

Figure A.6: Processed MT data for sounding chi004 from the Reykjanes high-temperature geothermal area. All measurements are functions of period. In the top to the left is the apparent resistivity and to the right is the phase angle. The second line to the left shows Zstrike for all periods and to the right are dimensionality variables, Skew, SkewB, Ellipticity and Coherency. These variables equal to zero for 1D and 2D structures. The last four figures correspond to Tipper. These data do not contain information on Tipper because vertical component of magnetic field, H_z, was not measured.